# A constitutive equation for thixotropic suspensions with yield stress by coarse-graining a population balance model

Paul M. Mwasame, Antony N. Beris, R. B. Diemer, Norman J. Wagner[1]

*Center for Molecular and Engineering Thermodynamics, Department of Chemical and Biomolecular Engineering, University of Delaware, Newark, DE 19716*

**Abstract**

A population balance model appropriate for the shear flow of thixotropic colloidal suspensions with yield stress is derived and tested against experimental data on a model system available in the literature. Modifications are made to account for dynamic arrest at the onset of the yield stress, in addition to enforcing a minimum particle size below which breakage is not feasible. The resulting constitutive model also incorporates a structural based relaxation time, unlike existing phenomenological models that use the inverse of the material shear rate as the relaxation time. The model provides a reasonable representation of experimental data for a model thixotropic suspension in the literature, capturing the important thixotropic timescales. When compared to prevalent structure kinetics models, the coarse grained population balance equation is shown to be distinct, emphasizing the novelty of utilizing population balances as a basis for thixotropic suspension modeling.

## 1. Introduction

Ideal thixotropy is defined as the continuous decrease of viscosity with time when flow is applied to a sample that has been previously at rest, and the subsequent recovery of viscosity when flow is discontinued [1]. In colloidal suspensions, the microstructure evolution thought to underly thixotropic behavior includes the formation of aggregates and even network structures that are associated with a yield stress [2]. These structures can undergo breakage under flow revealing the complex interplay between rheology and microstructure. Thixotropic suspensions are also inherently multiscale in nature, with multiple length scales leading to multiple time scales that also depend on the flow conditions. This explains much of the complex non-Newtonian rheological behavior, including hysteresis and viscoelasticity, observed in these systems [3, 4]. More detailed reviews on this subject are offered by Mewis [5], Barnes [6] and Mewis and Wagner [7].

Thixotropic media are frequently encountered in large-scale industrial processes including oil pipeline-transport, red-mud in minerals processing [8] and waste processing at superfund sites [9]. In addition, thixotropic agents are prominent in consumer applications, such as beauty creams [10], and have even been proposed for gelled hydrocarbon fuel applications [11]. Printing inks [12, 13] and even blood can be considered thixotropic [14]. The breadth and growing importance of these applications coupled with environmental concerns justifies the considerable effort put into developing predictive models for such systems. At the heart of these modeling efforts is the relationship between microstructure and rheology. Consequently, models incorporating microstructural variables are required to understand, interpret and predict rheological behavior of such systems.

[1]Corresponding Author: wagnernj@udel.edu

The earliest formal use of a structural variable to model the structural dynamics in a thixotropic suspension can be traced back to the work of Goodeve [15]. At the heart of this approach is the concept that structural changes govern the rheology of thixotropic suspensions, and these can be accounted for by tracking the creation and destruction of 'bonds' in the system. This 'structure kinetic' approach has been applied with some success in developing rheological constitutive equations for thixotropic suspensions [14, 16], but with limitations. The most glaring deficiency is the difficulty in unambiguously relating the order parameter describing creation and breakage of bonds to experimental measurements of the microstructure. Furthermore, the structure kinetic equations are phenomenological as they contain parameters that cannot be directly interpreted in terms of the properties of the suspension of particles. Therefore, it is desirable to develop new theoretical approaches that relate structural changes in a thixotropic suspensions to fundamental processes and properties at the particle level.

This work develops a macroscopic rheological model for thixotropic suspensions based on population balances [17, 18]. Our effort is aided by the extensive literature available on characteristic rate processes [19, 20, 21] and fractal scaling theories applicable to aggregating colloidal dispersions. Previous efforts have related the rheology of colloidal dispersions to microstructural changes through the use of population balances. von Smoluchowski [22] may have been the first one to connect colloidal aggregation to suspension viscosity. Barthelemes et al. [23] applied a coupling between a sectional population balance model and a rheological law to describe the viscosity of a flowing suspension. Mohtaschemi et al. [24] also applied a similar approach to describe the rheology of an aggregating colloidal suspension. All these studies point to the important role microstructure plays in determining the rheology of aggregating soft colloidal suspensions and the promise of population balances.

Despite the success of population balances in modeling the microstructure and rheology, these studies were limited to purely viscous suspensions and are not applicable to thixotropic suspensions with a yield stress. In this work we address the two main challenges in developing such a theory: 1) How to account for the dynamical arrest characterized as a yield stress; and 2) How to coarse grain the theory to yield an efficient model that retains sufficient connection between particle-level properties and emergent rheological behavior and free from unnecessary phenomenology. By applying appropriate model assumptions, different from the preceding works, we develop a coarse-grained, single variable, evolution equation that accounts for structural changes in thixotropic suspensions with a yield stress.

A constitutive equation is required to calculate the suspension rheology (shear stress) from the structural predictions arising from the coarse grained population balance equation. The formulation of a constitutive relationship for thixotropic suspensions remains an open question [7]. In this work a simple, phenomenological constitutive relationship that sums a structure-dependent viscous contribution and a structure-dependent elastic contribution is assumed. More generally, the coarse-grained population balance equation developed here can, in principle, be used in any existing constitutive model for thixotropy that incorporates an appropriate structural variable. Therefore, the focus of the present work is the development of a coarse-grained population balance model appropriate for thixotropic suspensions with yield stress. For the purposes of illustrating and validating the model, we use the recently published data set of Armstrong et al. [25] that expands upon the experimental data on a model system first proposed by Dullaert and Mewis [26]. This data set, available online, is for a thixotropic silica suspension and includes a broad range of rheological experiments including steady-state, transient step-up and step-down, flow reversal

and oscillatory shear experiments.

In the following, we begin with a brief description of the development of a population-based model for thixotropic suspensions experiencing shear flow. The coarse-graining of the population balance equation is then carried out through the moment method. Next, we address further modifications necessary to describe concentrated thixotropic suspensions that display a yield stress. A phenomenological constitutive relationship is then proposed to link the microstructural calculations arising from the population balance to the macroscopic stress that is measured in rheological experiments. The model parameterization is then described and subsequent validation is perfomed using a rheology dataset available in the literature [25]. The model predictions are discussed and tested against oscillatory shear and flow reversal experiments. Finally, the coarse-grained population balance equation is compared against the phenomenological structure kinetic one followed by a discussion of the main conclusions.

## 2. Theory

### *2.1. The population balance model*

In suspensions, aggregation of colloidal particles gives rise to fractal-like aggregate structures that exhibit self-similarity over multiple length scales [27]. These emerging additional scales make thixotropic suspensions challenging to model. However, by applying existing knowledge and appropriate theories describing aggregation and breakage at the particle level, we can build an approximate but detailed microscopic description of the evolution of suspension microstructure in shear flows. The starting point is the mass-fractal relationship that connects the size of the aggregate, $R_a$, and the number of primary particles in an aggregate, $m$, defined by

$$\frac{R_a}{a_p} = m^{1/d_f} \ , \tag{1}$$

where the aggregate size is normalized by the radius of the primary particles, $a_p$. These length scales are described schematically in Fig. 1. Note that the aggregates are assumed to be spherical on average and the fractal dimension is taken to be uniform, independent of size.

Next, we consider a univariate population of aggregates defined by $n(m)$, the number density of aggregates with $m$ to $m + dm$ primary particles per aggregate. The aggregate population is assumed to be randomly and homogeneously distributed in space, hence the spatial positions of aggregates in the flow field are not tracked. The population balance equation (PBE) [17, 18] describing the evolution of a population of aggregates under the influence of aggregation and breakage processes can be written as [28]

$$\begin{aligned}\frac{dn(m,t)}{dt} = \\ \frac{1}{2}\int_0^\infty [a(m-m',m';\dot\gamma) + c(m-m',m')]n(m-m',m')n(m')dm \\ - \int_0^\infty [a(m-m',m';\dot\gamma) + c(m-m',m')]n(m)dm \\ + \int_m^\infty b(m';\dot\gamma)P(m|m')n(m')dm' - b(m;\dot\gamma)n(m)dm \ ,\end{aligned} \tag{2}$$

where $a$ and $b$ are size and shear-dependent aggregation and breakage kernels respectively and $c$ is a Brownian kernel. These will be described shortly. $P(m|m')$ denotes the daughter distribution arising from fragmentation of aggregates of size $m'$ into smaller fragments of size $m$. Eq. 2 describes the time evolution of the density function, $n(m)$, of aggregates in an infinitesimal size class, $m$ to $m + dm$. The terms on the right hand side account for the rate of generation of size-$m$ aggregates due to the aggregation of smaller aggregates or the breakage of larger aggregates, as well as the rate of destruction of size-$m$ aggregates due to aggregation with other aggregates, or breakage into smaller ones.

The three rate kernels, $a$, $b$ and $c$, are now described. The

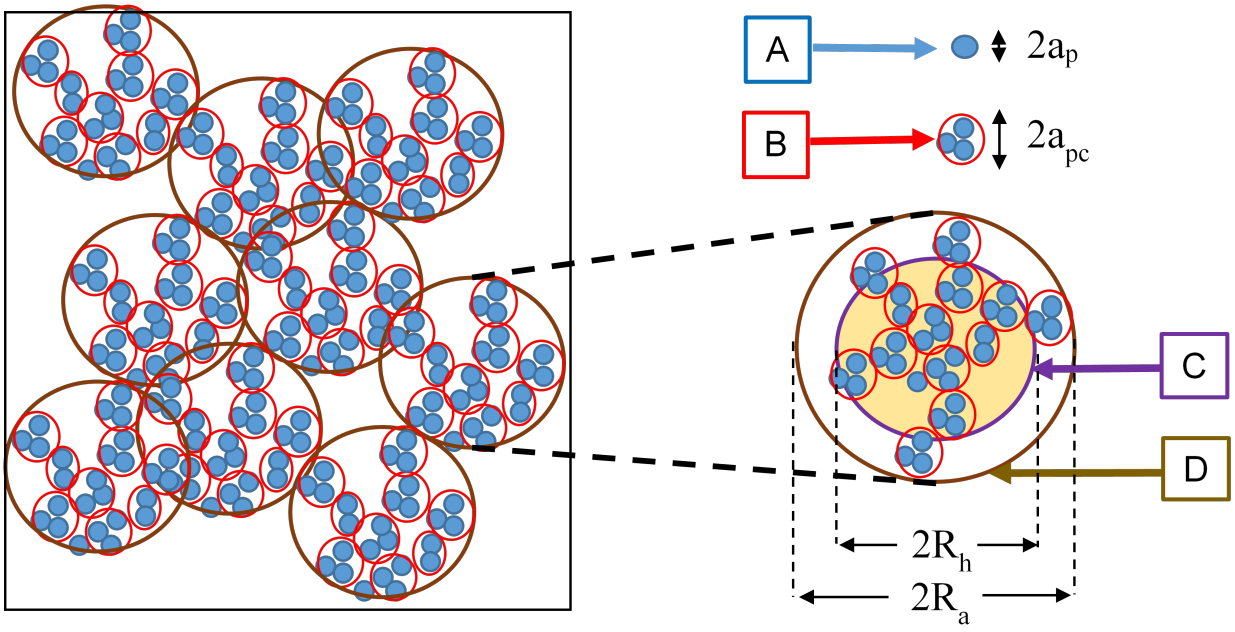


Figure 1: An illustration of the multiple length scales present in the aggregate network of a thixotropic suspension showing the primary particles of diameter $2a_p$ (A), primary clusters of diameter $2a_{pc}$ (B), viscometric volume of the aggregates characterized by diameter $2R_h$ (C) and an effective volume of the aggregates characterized by diameter $2R_a$ (D).

first is the rate of shear driven aggregation between aggregagtes of mass $m$ and $m'$, which was derived by von Smoluchowski [19] and is given by

$$a(m, m'; \dot{\gamma}) = \frac{4}{3}\alpha a_p^3 |\dot{\gamma}| \left(m^{1/d_f} + m'^{1/d_f}\right)^3 , \tag{3}$$

where $\dot{\gamma}$ is the shear rate and $\alpha$ is the collision efficiency. Next, the rate of Brownian aggregation, also derived by von Smoluchowski [19, 20], is given by

$$c(m, m') = \left(\frac{2k_B T}{3\mu_s W}\right)\left(m^{1/d_f} + m'^{1/d_f}\right)\left(m^{-1/d_f} + m'^{-1/d_f}\right) , \tag{4}$$

where $k_B$ is Boltzmann's constant, $T$ is the temperature in Kelvin, $\mu_s$ is the medium or solvent viscosity, $W$ is the Fuch's stability ratio [29] and $d_f$ is the fractal dimension. A detailed review of flocculation models is presented by Thomas et al. [30].

Two main approaches have been proposed in the literature to the describe the breakage rate kernel, $b$: exponential and power law kernels. The latter is used in this work. Particle breakage occurs when a stress acting on an aggregate exceeds its cohesive strength. One may consider two types of stresses that can cause breakage, (i) stresses induced by collisions and (ii) stresses caused by velocity gradients in the fluid [31]. In this work, we adopt a power law breakage kernel that casts the functional dependence of breakage frequency as a product of the size of aggregates and the shear rate that provides the driving force for breakup. Following Spicer and Pratsinis [21], the breakage rate of aggregates in a shear field is given by

$$b(m; \dot{\gamma}) = b_o |\dot{\gamma}|^2 m^{1/d_f} , \tag{5}$$

where $b_o$ is a pre-factor. Given Eq. 1, the breakage rate is assumed to depend linearly on the aggregate size.

*2.2. Coarse graining the population balance equation*

In practice, solving Eq. 2 using the auxilliary Eqs. 3-5 is not a simple task because it is an integro-differential equation and the rate processes depend on the mass $m$ of the aggregates. However, we do not necessarily require all the information present in the aggregate size distribution, $n(m)$. Therefore, the method of moments is used to extract only the relevant information needed from the aggregate size distribution [32, 33]. Still, the moment equations may constitute an open set of coupled equations owing to the non-linear aggregation and breakage rate processes in Eqs. 3-5. Therefore, additional coarse graining involving assumptions about the underlying aggregate size distribution must be performed to obtain an approximate but closed set of moment equations that are more useful for engineering applications [34].

The $k^{th}$ moment of the aggregate size distribution, $M_k$ , is defined by

$$M_k = \int_0^\infty m^k n(m) dm \ . \tag{6}$$

However, it is preferable to work in terms of the scaled aggregate size distribution, $\hat{n}(m)$, given by

$$\hat{n}(m)dm = \frac{n(m)dm}{N_0} \ , \tag{7}$$

where the normalization constant, $N_o$, is the total number of primary particles per unit volume in the suspension. The corresponding scaled moments, $\mu_k$, are then defined as

$$\mu_k = \frac{M_k}{N_0} = \int_0^\infty m^k \hat{n}(m) dm \ , \tag{8}$$

Physically, the zeroth scaled moment, $\mu_0$, represents the reciprocal of the average aggregation number while the first moment, $\mu_1$, is the total mass of primary particles, which is a conserved quantity in a closed system. It is readily observed that $\mu_0$ is a bounded quantity, taking on values between 0 and 1, while $\mu_1 = 1$ reflecting mass conservation. The set of scaled moment equations, equivalent to the PBE in Eq. 2, is given by

$$\begin{aligned} &\frac{d\mu_k(t)}{dt} = \\ &\frac{1}{2} N_o \int_0^\infty \hat{n}(\lambda) \int_0^\infty [a(\lambda,\epsilon) + c(\lambda,\epsilon)] \hat{n}(\epsilon) d\epsilon d\lambda \\ &- N_o \int_0^\infty m^k \hat{n}(m) \int_0^\infty [a(\lambda,\epsilon) + c(\lambda,\epsilon)] \hat{n}(\epsilon) d\lambda dm \\ &+ \int_0^\infty \lambda^k b(\lambda) \hat{n}(\lambda) d\lambda \, (\theta_k - 1) \ . \end{aligned} \tag{9}$$

The simplification in the last term of this equation is possible by assuming that the daughter distribution, $P(m|m')$, depends only on the relative ratio $\xi = m/m'$ [33]. Physically, self-similar breakage represents a scenario in which all aggregates possess the same daughter distribution regardless of the parent aggregate size. Such a self-similar daughter distribution is defined by $P(\xi)$ with moments, $\theta_k$, given by

$$\theta_k = \int_0^1 \xi^k P(\xi) \, d\xi \ . \tag{10}$$

As will be shown shortly in the coarse-graining, only the zeroth moment of the daughter distribution, $\theta_0$, physically representing the number of fragments formed during a breakage event, is required here. Therefore, the particular form of $P(\xi)$ does not need to be specified.

The rate kernels in Eqs. 3-5 together with Eq. 9, yield the following equations for the first three moments

$$\begin{aligned} \frac{d\mu_0}{dt} = &- \left( \frac{kT\phi_p}{2\mu_s W \pi a_p^3} \right) \left( \mu_0^2 + \mu_{-1/d_f} \mu_{1/d_f} \right) \\ &- \alpha |\dot{\gamma}| \left( \frac{\phi_p}{\pi} \right) \left( \mu_0 \mu_{3/d_f} + 3\mu_{2/d_f} \mu_{1/d_f} \right) \\ &+ b_o |\dot{\gamma}|^2 \mu_{1/d_f} \, (\theta_0 - 1) \ , \end{aligned} \tag{11}$$

$$\frac{d\mu_1}{dt} = 0 \ , \tag{12}$$

$$\frac{d\mu_2}{dt} = -\left(\frac{kT\phi_p}{2\mu_s W\pi a_p^3}\right)\left(2\mu_1^2 + 2\mu_{1+1/d_f}\mu_{1-1/d_f}\right) - \alpha|\dot{\gamma}|\left(\frac{\phi_p}{\pi}\right)\left(2\mu_1\mu_{1+3/d_f} + 6\mu_{1+2/d_f}\mu_{1+1/d_f}\right) + b_o|\dot{\gamma}|^2\mu_{2+1/d_f}\left(\theta_2 - 1\right) \ . \tag{13}$$

The volume fraction of the primary particles, $\phi_p$, enters the above equations through the following relationship

$$\phi_p = \frac{4}{3}\pi a_p^3 N_0 \ . \tag{14}$$

In the moment equations above, Eqs. 11 - 13, the stability ratio (W), collision efficiency ($\alpha$), breakage pre-factor ($b_o$), fractal dimension ($d_f$) and moments of the daughter distribution ($\theta_k$) are microscopic parameters. In principle, all of these parameters may be determined from independent experiments or theory as they represent physical properties of the particles and aggregates.

The resulting set of moment equations is not closed and also involves fractional moments. A closure rule is required to facilitate numerical solutions. The closure rule adopted in this work is that the population of aggregates is monodisperse at each step in its trajectory [35, 33]. This simple assumption is depicted in Fig. 2, and is represented mathematically as

$$\hat{n}(m) = \mu_0\delta\left(m - m_n\right) \ . \tag{15}$$

The additional variable $m_n$ appearing in the delta function above represents the average number of primary particles per aggregate, and is given by

$$m_n = \mu_1/\mu_0 = 1/\mu_0 \ . \tag{16}$$

The moments of the distribution described in Eq. 15 are

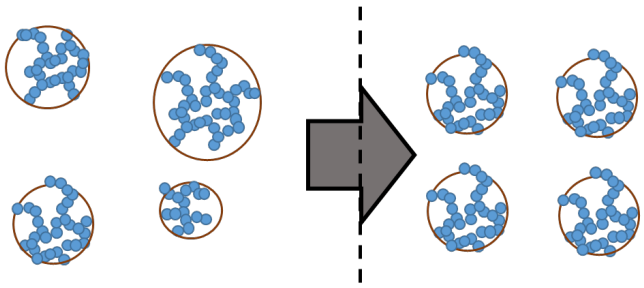

Figure 2: A physical representation of the monodisperse closure rule. The real system (left) is represented by an idealized system (right) in which the mass is distributed equally over all aggregates in the system.

given by

$$\mu_k = \int_0^\infty m^k \mu_0\left(m - m_n\right) dm = \mu_0 m_n^k = \mu_0^{1-k} \ . \tag{17}$$

This closure rule allows for the simplification of the infinite set of moment equations, Eq. 9, to a single dynamic equation for the zeroth moment

$$\frac{d\mu_0}{dt} = -2\left(\frac{kT\phi_p}{2\mu_s W\pi a_p^3}\right)\mu_0^2 - 4\alpha|\dot{\gamma}|\left(\frac{\phi_p}{\pi}\right)\mu_0^{2-3/d_f} + b_o|\dot{\gamma}|^2\mu_0^{1-1/d_f}\left(\theta_0 - 1\right) \ , \tag{18}$$

and an algebraic equation for all higher order moments

$$\mu_k = \mu_0^{1-k}\mu_1^k \ . \tag{19}$$

Eq. 18 describes the evolution of the reciprocal of the aggegation number $\mu_0$. The first term on the right hand side of Eq. 18 represents the effect of Brownian aggregation while the second and third represent shear aggregation and shear breakage respectively. The important outcome here is that the integro-differential population balance model can now be represented by a single ordinary differential equation for the zeroth moment. Furthermore, this closure rule eliminates the need to specify a particular daughter distribution, only requiring information on

the number of fragments produced during a breakage event $\theta_0$

The framework applied so far to describe aggregation and breakage kinetics of colloidal aggregates was originally derived for dilute suspensions [19] and has been successfully applied by multiple authors [21, 23, 35, 36] using the moment method. However, the structure dynamics in a concentrated thixotropic suspension strongly deviate from this idealized picture because fractal aggregates can fill space, leading to dynamic arrest and a yield stress. Therefore, the limitations of the underlying expressions used in this section now need to be examined and appropriate modifications made to extend their applicability to typical suspensions encountered in practice.

### *2.3. Modifications necessary for thixotropic suspensions with yield stress*

In this section we discuss some necessary improvements, albeit phenomenological and by no means unique, to ensure the evolution equation for the zeroth moment closely describes experimental observations.

#### *2.3.1. Incorporating dynamic arrest*

Suspensions of practical relevance are typically more concentrated [16, 37] than those studied by previous authors [21, 23, 35, 36]. This means we have to include additional physics into the rate processes describing aggregation and breakage processes. Rheological experiments on thixotropic suspension provide some guidance on how to do this. In particular, an important observation by Dullaert and Mewis [37] is that of a yield stress at finite shear viscosity. This means that the increase in hydrodynamic viscosity due to presence of aggregates alone is not sufficient to explain the dynamic arrest when a space filling network forms. Rather, a network elasticity due to percolation of the aggregates is what gives rise to the yield stress.

As aggregation proceeds, hydrodynamic interactions intensify noticeably [38]. To account for this, the aggregation rate should be calculated by considering that each aggregate exists in an effective medium of other aggregates. This is accomplished by replacing the medium viscosity, $\mu_s$, by the effective suspension viscosity, $\mu_s\eta_r^h$, in the Brownian aggregation kernel in Eq 4 resulting in

$$c(\lambda,\epsilon) = \left(\frac{2kT}{3\mu_s\eta_r^h W}\right)\left(\lambda^{1/d_f} + \epsilon^{1/d_f}\right)\left(\lambda^{-1/d_f} + \epsilon^{-1/d_f}\right) , \quad (20)$$

where $\eta_r^h$ is the relative viscosity of the suspension. Although many choices exist for describing the suspension viscosity [39, 40], the robust and simple Marron and Pierce [41] equation is used to define the relative hydrodynamic viscosity as

$$\eta_r^h = \left(1 - \frac{\phi_h}{\phi_{max}}\right)^{-2} . \quad (21)$$

In this expression, $\phi_h$ is the viscometric volume fraction of the porous aggregates while $\phi_{max}$ is the maximum packing fraction of the aggregates. Considering that a finite viscous contribution to the viscosity is observed when the space filling network forms [25], the hydrodynamic radius of the aggregate $R_h$ is smaller than the aggregate size $R_a$, i.e. the aggregates are porous to the fluid. If we define the aggregate volume fraction as

$$\phi_a = \phi_p\mu_0^{1-3/d_f} , \quad (22)$$

the viscometric volume fraction that enters the viscosity calculation in Eq. 21 may be approximated by

$$\phi_h = \left(\frac{R_h}{R_a}\right)^3 \phi_a , \quad (23)$$

where $R_h/R_a$ reflects the permeability of the fractal aggregates and is assumed to be constant. This completes the first modification to the Brownian aggregation rate kernel.

The porous nature of fractal aggregates means that the sus-

pension's hydrodynamic viscosity does not diverge so as to arrest perikinetic aggregation. Furthermore, at low shear rates, the shear aggregation term ($\sim \dot{\gamma}$) dominates the shear breakage term ($\sim \dot{\gamma}^2$), leading to a run-away increase in aggregate size. It is therefore possible for aggregates to grow to very large sizes, allowing the configurational aggregate volume fraction, $\phi_a$, to exceed $\phi_{max}$. Such predictions are unphysical. To remedy this, the emerging yield stress is identified as an independent constraint on the trajectory of growing aggregates that sets the maximum aggregate size. Mohtaschemi et al. [24] associated dynamic arrest of perikinetic aggregation with trapping of aggregates at high viscosities. They introduce a hyperbolic cutoff function that arrests brownian aggregation once the suspension viscosity exceeds a critical value $\eta_c$. In addition, their viscosity calculation assumes the aggregates are impermeable. Although, their approach is not directly applicable to dynamic arrest in thixotropic suspensions of porous fractal aggregates that exhibit a finite hyrodynamic viscosity and a yield stress [37], we can adapt the concept to our model.

Dynamic arrest in the presence of porous fractal aggregates is attributed to the increase in contact probability due to growth of aggregates, which stops further growth once a space filling network forms as $\phi_a$ approaches $\phi_{max}$. Thus the yielding behavior arises from elastic stresses. This aggregate jamming effect is modeled as an onset phenomenon by a hyperbolic cutoff function

$$\beta \equiv \beta(\phi_a(\mu_0)) = tanh\left(\chi \frac{\phi_{max} - \phi_a}{\phi_{max} - \phi_{pc}}\right) , \tag{24}$$

where $\beta$, $0 < \beta < 1$, is an effective factor weighting the aggregation kernels $a$ and $c$. The constant $\chi$ is assigned a value of 2.65, chosen such that $\beta$ approaches a value of 0.99 when all aggregates are broken down to their minimum allowable size characterized by a corresponding volume fraction $\phi_{pc}$. The evaluation of $\phi_{pc}$ is discussed later in this section. The order parameter $\left(\frac{\phi_{max}-\phi_a}{\phi_{max}-\phi_{pc}}\right)$ describes the proximity to the yield stress, while $\beta$ is applied as a pre-multiplier to the shear and Brownian aggregation kernels. This completes the modification of the aggregation processes.

### *2.3.2. Enforcing minimum breakage size*

Depending on the pre-shear/pre-processing protocol, the initial rest state of the suspension may consist of permanent aggregates of the constituent primary particles, referred to here as primary clusters, which in turn can combine to form larger aggregates depicted in Fig. 1. Primary clusters have been confirmed using small angle X-ray and neutron scattering [42, 43]. Rheologically, primary clusters are associated with a high shear rate viscosity that significantly exceeds the expected theoretical value based on the actual solids loading of the primary particles $\phi_p$. Therefore, a lower size bound must be enforced to ensure that the aggregates never break below their smallest, allowable size based on the suspension preparation protocol. Thus, at high shear rates, the breakage rate should tend to zero as the aggregates are broken down into their constituent primary clusters.

This requirement is enforced by modifying the breakage rate in Eq. 5 to

$$b(m) = b_o \dot{\gamma}^2 \left(m^{1/d_f} - m_p^{1/d_{fpc}}\right) , \tag{25}$$

where $m_p$ is the number of primary particles in the primary cluster. A value of $m_p = 1$, implies the aggregates can be broken down to the constituent primary particles of size $a$. The size of the primary clusters may be estimated as $a_{pc} = a_p m_p^{1/d_{fpc}}$, characterized by a second fractal dimension $d_{fpc}$. Finally, $\phi_{pc}$, is associated with the cluster volume fraction, and calculated as $\phi_{pc} = \phi_p m_p^{(3/d_{fpc}-1)}$. The fractal dimension of the primary cluster ($d_{fpc}$) is equal to the aggregate fractal dimension ($d_f$). This assumption can be relaxed if additional information about the

primary clusters is available.

### 2.3.3. Modified moment equation

To arrive at the modified set of moment equations we need to pre-multiply Eqs. 3 and 20 for the aggregation kernels by Eq. 24 and use the new expression for the breakage kernel provided by Eq. 25. These expressions are substituted into Eq. 9. By applying the monodisperse closure rule as described in Section 2.2, the evolution equation for the zeroth moment is given by

$$\begin{aligned}\frac{d\mu_0}{dt} =& -2\beta\left(\frac{kT\phi_p}{2\mu_s\eta_r^h W\pi a_p^3}\right)\mu_0^2 - 4\beta\alpha\left(\frac{\phi_p}{\pi}\right)|\dot{\gamma}|\mu_0^{2-3/d_f} \\ &+ b_o|\dot{\gamma}|^2\left(\mu_0^{1-1/d_f} - m_p^{1/d_{fpc}}\mu_0\right)(\theta_0 - 1)\ ,\end{aligned} \tag{26}$$

with all other moments provided by Eq. 19. Eq. 26 represents the evolution of microstructure in a thixotropic suspension with a yield stress while also allowing for the existence of primary clusters for $m_p \neq 1$. Next, a constitutive equation for the shear stress, incorporating $\mu_0$ as the microstructural variable, is specified to complete the model development.

## 2.4. Constitutive model for the shear stress

The rigorous development of an appropriate constitutive relationship for the stress tensor based on microscopic insights remains a challenge and is not addressed in this work. Rather, a semi-empirical expression for the shear stress is developed to interpret rheological data. More specifically, the constitutive relationship assumes that stress is given by a superposition of elastic and viscous, i.e. purely hydrodynamic, contributions [6, 16].

$$\sigma = \sigma_{elastic} + \sigma_{viscous}\ . \tag{27}$$

The structural variable, $\mu_0$, is linked to the various contributions to the macroscopic stress, $\sigma$, as follows. The viscosity of the aggregates is computed by assuming knowledge of the viscometric volume of the aggregates as described in Section 2.3.1. Subsequently, the viscous contribution to the shear stress is calculated as

$$\sigma_{viscous} = \mu_s\eta_r^h(\phi_h, \phi_{max})\,\dot{\gamma}\ , \tag{28}$$

where $\eta_r^h$ is given by Eq. 21.

Less insight is available about the elastic contribution to the shear stress and few, well developed micromechanical models are available [44, 45, 46]. Instead, following Armstrong et al. [25] and Apostolidis et al. [14], the macroscopic elastic stress due to deformation of interacting aggregates is expressed as the product of a structure dependent modulus ($G(\phi_a)$) and elastic strain ($\gamma_e$) as

$$\sigma_{elastic} = G(\phi_a)\,\gamma_e(\phi_a)\ . \tag{29}$$

The only constraint we impose on the form of $G(\phi_a)$ is the ability to recover the limiting expressions of Shih et al. [47] at equilibrium i.e., as $\phi_a$ approaches $\phi_{max}$. The elastic modulus depends on the level of structure as

$$G(\phi_a) = G_o\left(\frac{\phi_a - \phi_{pc}}{\phi_{max} - \phi_{pc}}\right)^{\frac{2}{3-d_f}}\ . \tag{30}$$

$G_o = G_{eq}\phi_p^{\frac{1}{3-d_f}}$ expresses the dependence of the effective equilibrium gel modulus, $G_{eq}$, on the total solids loading as described by Shih et al. [47]. The $\phi_a$-dependent term in Eq. 30 accounts for the effect of aggregation and breakage on the microstructure.

The elastic strain in the material at any moment is assumed to obey an evolution equation defined based on [48] as

$$\frac{d\gamma_e}{dt} = \left(\dot{\gamma} - \frac{\gamma_e}{\tau}\right)\ . \tag{31}$$

There are a number of ways to specify the relaxation time $\tau$. For

example, a number of investigators have employed kinematic hardening theory [14, 25, 48] leading to

$$\tau = \frac{\gamma_{lin}}{|\dot{\gamma}|} \ . \tag{32}$$

In this expression, $\gamma_{lin}$ is the limit of linearity of the material that is determined from creep or oscillatory strain sweep experiments. The shortcoming of Eq. 32 is that on changing the shear rate, the relaxation time also changes instantaneously.

A well-posed relaxation time should remain at its previous value, $\tau$, at the instant the shear rate is changed, before evolving to its final value at the new shear rate. To fulfill this requirement, $\tau$ may be specified through a dependence on the 'structural shear rate', $\dot{\gamma}(\phi_a)$, as

$$\tau = \frac{\gamma_{lin}}{\dot{\gamma}(\phi_a)} \left| \frac{\gamma_{lin}}{\gamma_e} \right| \ . \tag{33}$$

$\dot{\gamma}(\phi_a)$ may be determined as the steady state solution of the shear rate in Eq. 26, by setting $\frac{d\mu_0}{dt} = 0$, as

$$\begin{aligned} \dot{\gamma}(\phi_a) =& \frac{B + \left| \sqrt{(B^2 + 4AC)} \right|}{2A} \\ & with \\ A =& b_o \left( \mu_0^{1-1/d_f} - m_p^{1/d_{fpc}} \mu_0 \right) (\theta_0 - 1) \\ B =& 4\beta\alpha \left( \frac{\phi_p}{\pi} \right) \mu_0^{2-3/d_f} \\ C =& 2\beta \left( 4 \frac{kT\phi_p}{2\mu\eta_r^h W\pi a_p^3} \right) \mu_0^2 \ , \end{aligned} \tag{34}$$

The concept of a structural shear rate represents an improvement over previous models that employ Eq. 32 and now allows us to better describe (visco)elastic effects seen in describe step-up, step-down and stress relaxation transients.

The final expression describing the total shear stress in a thixotropic suspension with a yield stress is

$$\sigma = G(\phi_a)\, \gamma_e(\phi_a) + \mu_s \eta_r^v(\phi_h, \phi_{max})\, \dot{\gamma} \ . \tag{35}$$

It is important to note that the elastic contribution to the stress depends on $\phi_a$ while the viscous contribution depends on $\phi_v$. This distinction indicates the respective microstructural origins of these two contributions.

### *2.5. Summary of model equations*

The full set of equations defining the coarse grained population balance model for thixotropic suspensions are:

(1) The constitutive relationship for the stress in Eq. 35,

$$\sigma = G(\phi_a)\, \gamma_e(\phi_a) + \mu_s \eta_r^h(\phi_h, \phi_{max})\, \dot{\gamma} \ .$$

with Eqs. 21, 30 and 31.

(2) The structure evolution equation for the zeroth moment in Eq. 26,

$$\begin{aligned} \frac{d\mu_0}{dt} =& -2\beta \left( \frac{kT\phi_p}{2\mu_s \eta_r^h W\pi a_p^3} \right) \mu_0^2 - 4\beta\alpha \left( \frac{\phi_p}{\pi} \right) |\dot{\gamma}| \mu_0^{2-3/d_f} \\ & + b_o |\dot{\gamma}|^2 \left( \mu_0^{1-1/d_f} - m_p^{1/d_{fpc}} \mu_0 \right) (\theta_0 - 1) \ . \end{aligned}$$

(3) The elastic strain given by Eq. 31

$$\frac{d\gamma_e}{dt} = \left( \dot{\gamma} - \frac{\gamma_e}{\tau} \right) \ .$$

with $\tau$ defined by Eq. 33.

Finally, the auxilliary variables appearing in these equations are given by:

(i) The relationship between the configurational volume and the zeroth moment in Eq. 22,

$$\phi_a = \phi_p \mu_0^{1-3/d_f} \ .$$

(ii) The relationship between the configurational volume

and viscometric volume in Eq. 23,

$$\phi_h = \left(\frac{R_h}{R_a}\right)^3 \phi_a \ .$$

## 3. Results and Discussion

### 3.1. Determining model parameters

The model has 13 parameters that need to be specified as listed Table 1 . Of these, 7 are termed *input* parameters because they can be determined based on physical arguments, theory or specific features of rheological experiments. The remaning 6 are *fit* parameters determined by global fitting of the model to appropriate rheological data. Although some of these parameters may be determined apriori from theory, owing to lack of complete information on the physicochemical properties of the constituents of the suspension, they are considered fit parameters. The specification of the model parameters is now demonstrated by considering a thixotropic suspension studied by Armstrong et al. [25].

#### 3.1.1. Input parameters

The primary particle volume fraction of the suspension (or total solids loading), $\phi_p$, is 0.03, the size of the primary particles, $a_p$, is 8 nm and the medium viscosity, $\mu_s$, is 0.41 Pa-s as reported by Armstrong et al. [25]. These three system parameters depend on the suspension formulation. Next, the yield stress, $\sigma_{y,0}$, and equilibrium modulus, $G_o$, are estimated from limiting rheological behavior to be 11 Pa and 450 Pa respectively following the approach outlined in [25]. Based on these two values, $\gamma_{lin}$ is computed as the ratio $\sigma_{y,0}/G_o = 0.024$, which agrees with independent measurements [25]. The remaining parameters are selected based on heuristics as follows. Under the assumption of binary breakage events, the zeroth moment of the daughter distribution, $\theta_0$ , is specified to be equal to 2. This means on average aggregates in the shear field breakup into two smaller particles. Finally, the maximum packing fraction, $\phi_{max}$, is taken as 0.64 [39] equal to random close packing.

#### 3.1.2. Fit parameters

The remaining 6 parameters ($W$, $\alpha$, $b_o$, $d_f$, $R_h/R_a$ and $m_p$) are fit to rheological data by an optimization algorithm [49]. Fortunately, some of these parameters may be constrained based on theoretical considerations. Values of $\alpha \leq 1$ are expected based on physical arguments regarding the efficiency of shear collisions [50]. The effective aggregate porosity, $R_h/R_a$, is related to aggregate structure through the fractal dimension [51, 52, 53], but is taken as a fitting parameter in this work. Its value is not expected to exceed 1, the single sphere limit of this measure. On the other hand $1.8 \leq d_f \leq 2.5$, where the limits on the fractal dimension correspond to diffusion limited aggregation [54] and shear mediated aggregation, respectively [55]. The stability ratio $W$ is restricted to be larger than 1 during the fitting procedure (alternatively, the theoretical value of W may also be determined from knowledge of the interparticle potential [29, 56, 57]). The breakage rate constant, $b_o$, is the least well understood parameter and is simply constrained to be positive. As a comparison, a successful structure kinetics model, the Modified Delaware Thixotropic Model (MDTM) model [25], has 8 fit parameters. However, unlike such phenomenological models, all the parameters in the population based model here have a physical meaning and can be determined independently.

#### 3.1.3. Fitting procedure

At a minimum, the model must be fit to at least one steady-state data set and at least one set of transient data to to estimate the parameters. In this work, a total of 14 sets of experimental data comprising of steady-state, step-up and step-down transient rheology data are used in fitting the remaining 6 parameters resulting in an overdetermined optimization problem. An objective function is used to determine the best fit of the the

model to the experimental data. The objective function used to carry out the regression is defined in [25] by

$$F_{objective} = \sum_{m=1}^{M} \frac{1}{N_m} \sum_{i=1}^{N_m} \frac{1}{P_k} \left| \frac{\sigma_{i,exp} - \sigma_{i,model}}{\sigma_{i,exp}} \right| , \qquad (36)$$

where $\sigma_{i,exp}$ the corresponding experimentally measured stress, $\sigma_{i,model}$ the stress calculated from the model, $N_m$ corresponds to the number of experimental data sets and $P_k$ denotes the number of data points in a given experimental data set.

A parallel simulated annealing algorithm described by Amstrong et al. [49] was used to fit the model parameters. This technique enables the determination of confidence intervals around the parameters by running multiple fits with different initial conditions. For this work, 15 randomly initialized runs, each with a different initial guess of the parameters, are performed to obtain average values of the best parameters and the associated 90% confidence intervals. In Table 1, the best fit values, with the smallest objective function value, do not always lie within the 90% confidence interval. This occurs since the algorithm converges to solutions characterized by larger values of $m_p$ and $d_f$ compared to the best fit value as shown in the supplemental section. On the other hand, the model is not very sensitive to the value of the stability ratio explaining why the best fit value of this parameter falls outside the 90% confidence interval. In the following, the overall best fit values are used for discussion while select statistics of the fit parameters are provided and discussed in the supplemental material.

### *3.2. Discussion of model fits*

The best fit parameter values are summarized in Table 1 and correspond to the smallest objective function value of 0.014, selected from the 15 independent runs. The stability ratio $W$ is found to be 4.08 while the value of $\alpha$ is determined to be 0.61, which is consistent with an expected repulsive interaction between silica primary particles. Furthermore, the fit value for $R_h/R_a$ of 0.92 is consitent with a more densely packed aggreagte structure. The fit value for $d_f$ is 2.11, which is also consistent with orthokinetic aggregation [55] while $m_p$ is 468 primary particles, which defines the primary clusters. The fit value of $b_o$ is 0.0084 s. This value of $b_o$ compares favorably with collision frequncies of $b_o = 0.0047$ s$^{0.6}$ reported by Spicer and Pratsinis [21] using a breakage kernel of the form $b_o|\dot{\gamma}|^{1.6}m^{1/3}$ (compared to ours given by $b_o|\dot{\gamma}|^2 m^{1/d_f}$). Although the breakage kernel has been the subject of research, [58, 59, 60], its theoretical development remains an ongoing area of research [61]. In the following, some representative results corresponding to the optimum set of parameters in Table 1 are discussed.

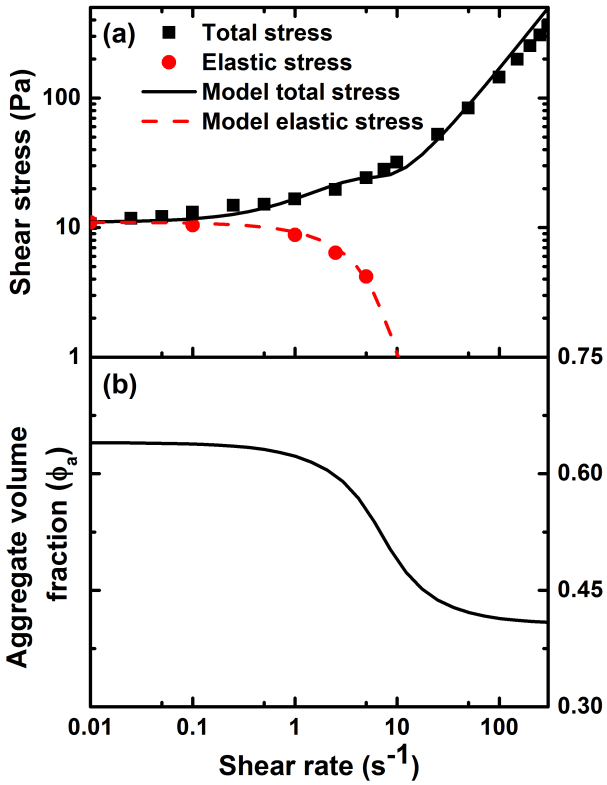


Figure 3: Model fits of shear stress as a function of shear rate compared against experimental data. Lines indicate fits to experimental data. Right hand axis indicates corresponding changes in aggregate volume fraction as a function of shear rate.

The model fit to the steady-state flow curve is presented in Fig. 3(a) showing good agreement with experimental data. The

Table 1: Summary of structural parameters in population based model. Optimized fit parameters are determined from simulated annealing parameter optimization annealing. See Section 3.1 for detailed discussion.

| Parameter | Symbol | Parameter type | Typical Range | Best Value | Average value | Units |
|---|---|---|---|---|---|---|
| Particle volume fraction | $\phi_p$ | System | $\leq \phi_{max}$ | 0.03 | - | - |
| Primary particle radius | $a_p$ | System | nm-$\mu$m | 8 | - | nm |
| Medium viscosity | $\mu_s$ | System | $\leq 1$ | 0.41 | - | Pa-s |
| Equilibrium modulus | $G_o$ | Empirical | $> 1$ | 450 | - | - |
| Yield stress | $\sigma_{y,0}$ | Empirical | $\leq 100$ | 11 | - | Pa |
| Number of daughter fragments | $\theta_0$ | Heuristic | $\geq 1$ | 2 | - | - |
| Maximum packing fraction | $\phi_{max}$ | Heuristic | $0.54 - 0.64$ | 0.64 | - | - |
| Stability ratio | $W$ | Optimized fit | $> 0$ | 4.08 | 50.78±14.12 | - |
| Collision efficiency | $\alpha$ | Optimized fit | $\leq 1$ | 0.61 | 0.70±0.086 | - |
| Breakage coefficient | $b_o$ | Optimized fit | $\geq 0$ | 0.0084 | 0.012±0.0035 | s |
| Aggregate fractal dimension | $d_f$ | Optimized fit | 1.8 - 2.5 | 2.11 | 2.21±0.03 | - |
| Cluster particle number | $m_p$ | Optimized fit | $\geq 1$ | 468 | 6814±3220 | - |
| Porosity | $R_h/R_a$ | Optimized fit | $\leq 1$ | 0.92 | 0.89±0.014 | - |

transition from the characteristic yield stress behavior at low shear rates to the viscous Newtonian behavior at high shear rates is well described by the model. The purely elastic contributions to the total stress, as determined from stress-jump experiments [25, 37], are also well described. This provides some empirical evidence that the stress in this suspension may be decomposed into elastic and viscous contributions as provided in Eq. 27. In the limit $\phi_a = \phi_{max}$, a yield stress is observed in the rheology while in the limit of $\phi_a = \phi_{pc}$ the shear thinning reaches the viscosity plateau for $\dot{\gamma} \geq 100$ s$^{-1}$. In these experiments, the elastic strain (not shown) is constant over all shear rates as these are steady shear experiments and the elastic strain in the microstructure is at its maximum value with $\gamma_e = \gamma_{lin}$. This result corresponds to the steady state solution of Eq. 31. Consequently, the decrease in elastic stress with increasing shear rate in Fig. 3 is attributable to the dependence of the elastic modulus on the aggregate volume fraction (see Eq. 30) which in turn depends on the shear rate, shown in Fig. 3(b). At $\dot{\gamma} \geq 1$ s$^{-1}$ the decrease in the magnitude of the elastic stress signals a reduction in the aggregate size and hence, aggregate volume fraction, as the breakage increasingly dominates. The good agreement between the measured and calculated elastic contributions to the shear stress also suggests that the yield stress is generated by a network elasticity at a finite viscosity.

The population balance model makes quantitative predictions for the microstructure under steady flow as shown in Fig. 3(b). The aggregate volume fraction ranges from 0.64 ($\phi_{max}$) at low shear rate to 0.38 ($\phi_{pc}$) at high shear rates. As the primary particles are conserved, this indicates that the aggregates are larger at lower shear rates than at higher shear rates. This can be explained by the fact that viscous stresses at high shear rates lead to aggregate break up, which is a consequence of the higher order dependence on the shear rate in the breakage kernel in Eq. 5 as compared to the shear aggregation kernel in Eq. 3.

The aggregate sizes under flow can be calculated using the fit value of the fractal dimension $d_{fpc} = d_f = 2.11$, with the primary cluster size, $a_{pc}$ determined to be 147 nm. The primary cluster is about 18 times larger in size than the primary particles ($a_p$=8 nm) and this result is consistent with experimental observations of permanent aggregates at the highest shear rates probed [42, 43]. In Fig. 4 the relative sizes of the aggregates as a function of shear rate, obtained from the following equation:

$$R_a/a_p = \frac{1}{\mu_0^{1/d_f}}, \tag{37}$$

are summarized for steady state conditions. The validity of this calculation may be independently verified through optical measurements by employing light or neutron scattering (see for example [43]).

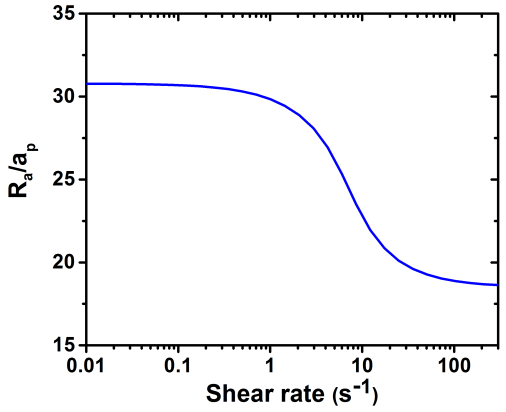


Figure 4: The calculated relative aggregate size as a function of shear rate using Eq. 37 where $a_p$ = 8nm is the primary particle radius.

Thixotropic behavior arises from the kinetics of aggregation (and/or breakage) processes. These can be probed by imposing a sudden change in shear rate on the suspension. Step-down experiments comprise of suddenly changing the shear rate at time t=0 from a steady-state value at t<0 to a new, lower shear rate at t=0 while tracking the evolution of the shear stress as a function of time. If a suspension is initially at steady state at a shear rate of 5 $s^{-1}$ (see Fig. 3) and at time t=0, the shear rate is suddenly changed to 1 $s^{-1}$, the behavior of the real suspension and model fits are as presented in Fig. 5. Prior to the step down to 1 $s^{-1}$, the total shear stress in the suspension and the elastic contribution are inidicated as $\sigma_{T,i}$ and $\sigma_{E,i}$ respectively. The difference between these two values is the viscous contribution to the shear stress labelled $\sigma_{V,i}$. Once the shear rate is suddenly reduced to 1 $s^{-1}$, the viscous contribution to the stress ( $\sigma_{V,f}$) immediately drops while the elastic stress ($\sigma_{E,f}$) slowly decreases following the relaxation behavior of the elastic strain as governed by Eqs. 31 and 33. At very short times t<0.1 s, the elastic modulus remains unchanged as the aggregate volume fraction is not changing as well and the elastic strain only changes due to the relaxation provided by Eq. 33. At t>0.1 s, the aggregate volume fraction begins to increase as aggregation is increasingly favored over breakage at smaller shear rates. This leads to two effects in the constitutive relationship. First, as $\phi_a$ increases, the viscosity increases and consequently, $\sigma_{V,f}$ increases as a function of time before reaching a steady state. Secondly, the changes in $\phi_a$ alter the relaxation time in Eq. 33 leading to the loading of elastic strain. In addition, the elastic modulus in Eq. 30 also increases as the aggregate volume fraction increases. It is important to note that while $\sigma_{V,i}$>$\sigma_{E,i}$, following the step down in shear rate, $\sigma_{E,f}$>$\sigma_{V,f}$ indicating the

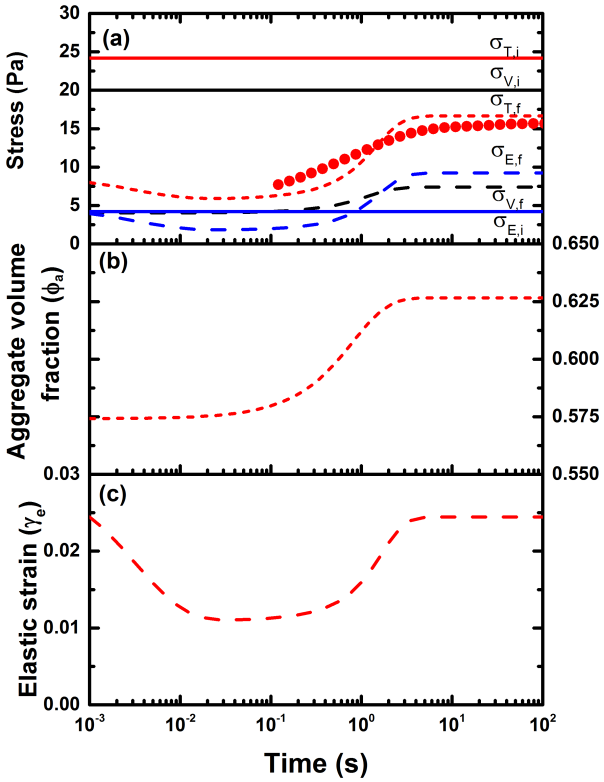


Figure 5: Model fits to a single step-down experiment where the initial shear rate is 5 $s^{-1}$ and at time t=0 the shear rate is suddenly changed to 1 $s^{-1}$. Total stress=red lines, viscous stress=black lines and elastic stress=blue lines. Experimental data in filled circles. (a) Solid lines indicated the initial steady-statae values prior to step-down, i.e. at 5 $s^{-1}$, of the total stress (T), viscous (V) and elastic (E) constributions indicated using subscript i. Dashed lines indicate evolution of the same measures as a function of time following the step down and respective contributions labelled using subscript f. (b) Structural predictions of the aggregate volume fraction as a function of time. (c) The evolution of the elastic strain as a function of time.

role of the percolating network's elastic stress in dominating the shear behavior at low shear rates. A key point here is that thixotropic signatures manifest in $\sigma_{T,f}=\sigma_{E,f}+\sigma_{V,f}$ are clearly correlated to the time evolution of $\phi_a$ or alternatively $\mu_0$.

A complete set of the fits to a series of step-down transient experiment are presented in Fig. 6(a). The model captures the general trends seen in the experimental results. In particular, the model is able to capture the thixotropic time scales along with their dependence on shear rate. During a step down experiment, from Fig. 6(b), we can observe that $\phi_a$ is an increasing function of time. This indicates that the aggregates grow larger when subjected to a much lower shear rate than the previous steady shear rate. Consequently, they occupy a larger volume of the space owing to their fractal nature. In addition, for all shear rates, we also observe from Fig. 6(c) that at short times (<0.1 s) some of the elastic strain relaxes from the previous value $\gamma_e = \gamma_{lin}$ before subsequently recovering back to final steady state value, $\gamma_{lin}$. This reflects the viscoelastic nature of the elastic stress behavior and is a consequence of the structural shear rate used in the definition of the relaxation time in Eq. 33.

In the step down experiment to 0.1 $s^{-1}$ in Fig. 6(a), it appears that the model predicts changes on longer timescales than those observed experimentally. On the other hand, in Fig. 6(b), it is evident that the evolution of $\phi_a$ occurs on the timescale of the experimentally measured stress. There is no explicit requirement that $\gamma_e$ must evolve on the same timescale as $\phi_a$ since in reality restructuring events may continue to occur over much longer timescales. Nevertheless, the discrepancy between experimental and model stresses suggests that the evolution equation of $\gamma_e$ needs to be reconsidered so as to better capture experimental timescales. In the supplemental section, possible modifications to improve the behavior of $\gamma_e$ leading to better agreement with experimental data are discussed. Ultimately, the key point here is that the evolution of $\phi_a$ occurs on the same timescale as that of the experimentally measured stresses showing the two are related. The model was also fit to analogous step-up experiments with similar success in capturing the thixotropic timescales (see supplemental information).

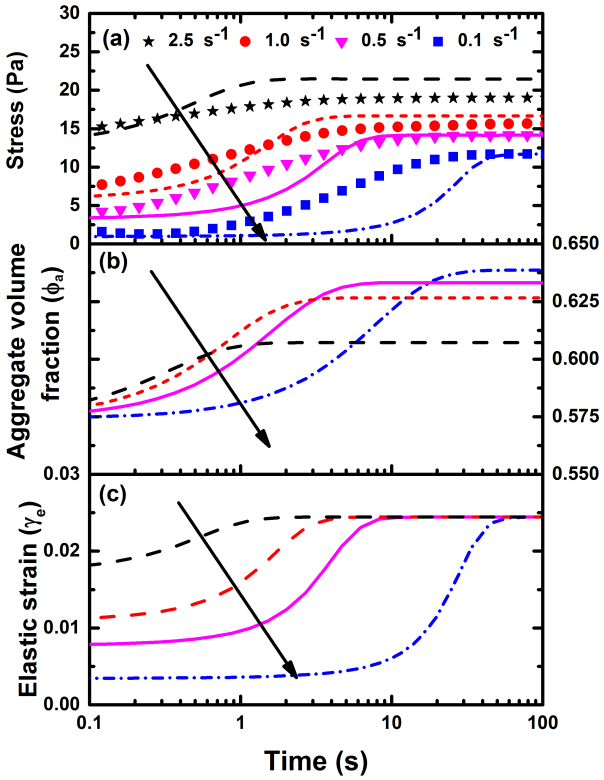


Figure 6: Model fits to step-down experiments. The initial shear rate is 5 $s^{-1}$ and at time t=0 the shear rate is changed to the final values indicated on the graph. In all cases, arrows indicate direction of decreasing final shear rate. (a) Shear stress as a function of time for step-down transient experiments. (b) Structural predictions of the aggregate volume fraction as a function of time. (c) The evolution of the elastic strain as a function of time.

### *3.3. Predictions of flow reversal, LAOS and UDLAOS*

The experiments described so far represent unidirectional shear flows. In practice, a suspension may be subjected to flows that involve a change in the direction of shear. Such experiments allow us to examine the elastic contributions to the shear stress as the viscous contributions do not depend on the direction of the shear.

Consider a flow reversal experiment in which a suspension is first allowed to attain steady state under shear in one direc-

tion. Then, at time t=0, the shear direction is suddenly changed to the opposite direction and the resultant stress measured. The corresponding model predictions are presented in Fig 7 and compared to the experimental data by Armstrong et al. [25]. In the flow reversal experiments at 1 $s^{-1}$ shown in Fig. 7(a), the shear stress gradually evolves from a positive value to negative when the shear rate is suddenly changed to -1 $s^{-1}$. If the shear stress was purely viscous, it would instantaneously become negative and take the same magnitude as in the prior direction since this contribution is proportional to the shear rate. Therefore, the complex time evolution of the stress can be attributed to the elastic stress arising from particle interactions in the sytem. These interactions are clearly directional in nature. The flow reversal experiments at higher shear rates exhibit similar trends albeit are always negative. This reflects the fact that viscous contributions dominate the total stress owing to the presence of broken down structures at higher shear rates. The aggregate volume fraction $\phi_a$ (Fig. 7(b)) remains unchanged over the duration of the experiment despite the complex material stress response. The zeroth moment, and therefore $\phi_a$, is an isotropic variable, and depends only on the magnitude of the shear rate. On the other hand, the elastic strain shown in Fig. 7(c) exhibits transient behavior and changes from positive to negative, reflecting the change in direction of shear and capturing the anisotropy inherent in thixotropic materials of interacting soft aggregates.

Amstrong et al. [25] also carried out LAOS experiments in which a sinusoidally varying strain rate is applied to a sample and the stress response is measured. The shear (strain) rate in LAOS is calculated from the frequency ($\omega$) and amplitude ($\gamma_o$) of the imposed oscillation as

$$\dot{\gamma(t)} = \gamma_o \omega cos\,(\omega t)\,, \tag{38}$$

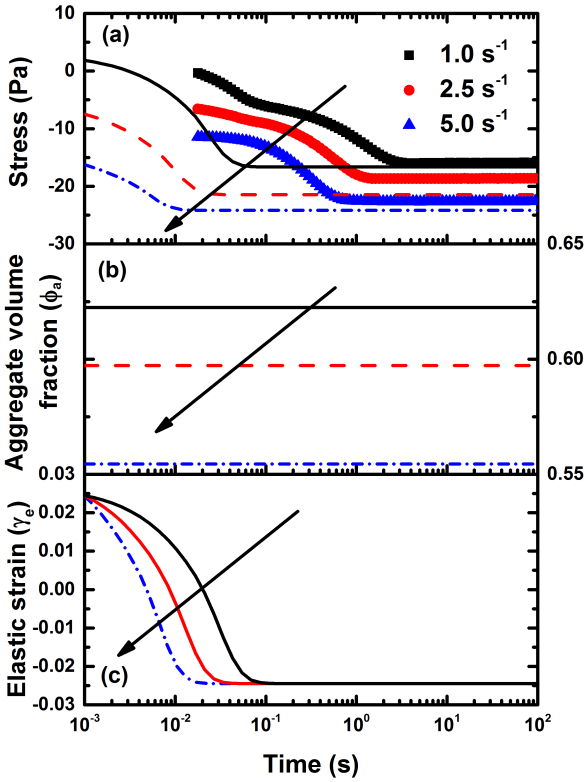


Figure 7: Model fits to flow reversal experiments. In all cases, arrows indicate direction of increasing magnitude of shear rate at which flow reversal experiment is conducted. (a) Shear stress as a function of time for flow reversal experiments. (b) Structural predictions of the aggregate volume fraction as a function of time. (c) The evolution of the elastic strain as a function of time.

and the associated strain amplitude imposed is given by,

$$\gamma(t) = \gamma_o sin\,(\omega t)\,. \tag{39}$$

$\gamma$ is the macroscopically imposed strain and is distinguished from the strain in the microstructure $\gamma_e$ defined by the model. The experimentally measured LAOS stress response and corresponding model predictions for $\omega = 0.1$ $s^{-1}$ and $\gamma_o = 10$ are summarized in Figs. 8. These correspond to viscous Lissajous projections of the stress response in a material state of steady alternance which is characterized by a periodic and stationary stress response (the complementary elastic Lissajous projection is presented in the supplemental section). From these results, the model captures the salient features observed in the LAOS

stress response data. In the viscous Lissajous projection in Fig. 8(a) there is a residual elasticity at $\dot{\gamma}$=0 that results in a non-zero shear stress that is also reflected in the elastic strain in Fig. 8(c). A purely viscous material would display zero stress at zero shear rate.

Under the experimental LAOS conditions, there is minimal change in the structure evidenced by the changes in $\phi_a$ shown in Fig. 8(b) and the elastic stress comprises the majority of the total stress as depicted in Fig. 8(a) (see dashed lines). Despite $\phi_a$ being close to the maximum packing fraction, the hydrodynamic viscosity is still comparatively low owing to the porosity of the fractal aggregates. At the largest magnitudes of the shear rate, $\phi_a$ attains its smallest value over the LAOS cycle indicative of the effect of shear in breaking down structure. The occurrence of the maximum value of $\phi_a$ at a shear rate magnitude of approximately 0.3 is indicative of the role of shear in enhancing aggregation at small values before breakage events begin to dominate at higher shear rates. The elastic strain imbues the model with a directionality allowing for predictions of shear stress when the direction of the shear rate changes in a LAOS experiment. The overshoot in shear stress seen in both the model and experimental data correlates well with the overshoot in $\phi_a$ and $\gamma_e$, in Figs. 8(b) and 8(c) respectively, indicating the occurence of the largest viscous and elastic stress contributions during a LAOS cycle. Other features predicted by the model are also seen in the experiment such as the double cross over in the stress response in the viscous Lissajous projection in Fig. 8(a). This feature originates from the evolution of the elastic strain (see Fig. 8(c)). A complete set of viscous and elastic projections comparing experimental and calculated model stress responses at multiple frequencies and strain amplitudes is presented in the supplemental section.

Finally, the model is also able to predict unidirectional LAOS (UD-LAOS) experiments. These are LAOS experiments with a

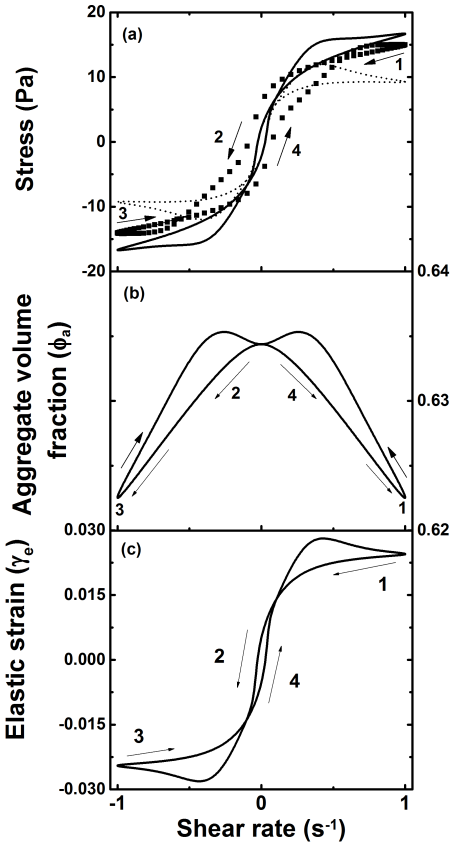


Figure 8: Viscous-Lissajous projections of the LAOS response of the model compared against experimental data at a frequence $\omega$=0.1 s$^{-1}$ and strain amplitude $\gamma$=10. (a) Model predictions showing the shear stress as a function of time in oscillatory strain rate compared against experimental data. Dashed lines indicate elastic constribution to stress while solid lines indicate total stress (b) Corresponding structural predictions of the aggregate volume fraction as a function of strain rate in oscillatory shear experiments. (c) The evolution of the elastic strain as a function of time in response to oscillatory strain rate.

background flow such that the shear rate is always constrained to be positive and described instead

$$\dot{\gamma}(t) = \gamma_o \omega cos\,(\omega t) + \gamma_o \omega = \Delta\dot{\gamma} + \gamma_o \omega. \tag{40}$$

Analogously, the shear strain is computed from

$$\gamma(t) = \gamma_o sin\,(\omega t) + \gamma_o \omega t. \tag{41}$$

The UD-LAOS experiment is characterized by a shear rate that is always positive or zero. The smallest value of the shear stress occurs at the smallest shear rate corresponding to $\Delta\dot{\gamma}$=-10 s$^{-1}$. In Fig. 9(b), the value of $\phi_a$ attains its maximum during a single

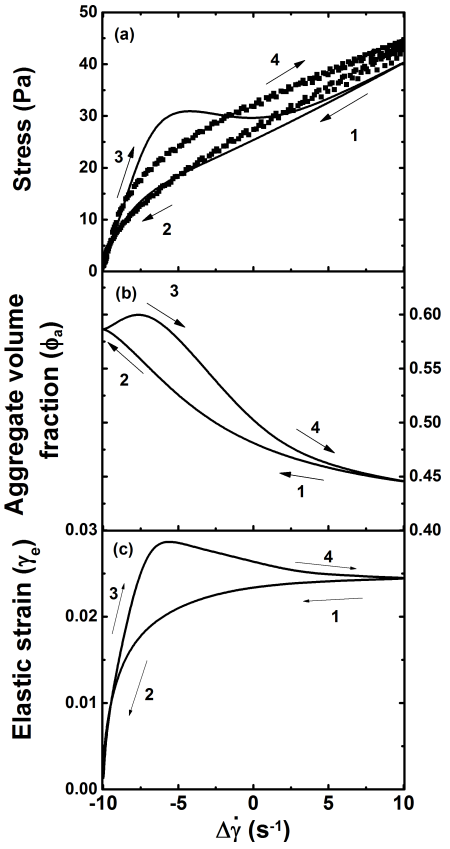


Figure 9: Viscous-Lissajous projections of the UD-LAOS response of the model compared against experimental data at a frequence $\omega$=1 $s^{-1}$ and strain amplitude $\gamma$=10. Results correspond to a period of steady alternance. The oscillatory strain rate is defined by $\Delta\dot{\gamma} = \dot{\gamma(t)} - \gamma_o\omega$. (a) Model predictions showing the shear stress as a function of time in oscillatory strain rate compared against experimental data. (b) Corresponding structural predictions of the aggregate volume fraction as a function of strain rate in oscillatory shear experiments. (c) The evolution of the elastic strain as a function of time in response to oscillatory strain rate.

period of oscillation at a value of $\Delta\dot{\gamma}$=-7.5 $s^{-1}$. This can be explained by the fact that shear facilitated collisions can also promote the aggregation rate beyond the Brownian rate. Therefore, at low shear rates, the rate of aggregation is enhanced leading to the peak in $\phi_a$ at $\Delta\dot{\gamma}$=-7.5 $s^{-1}$. At higher shear rates, the breakage rate begins to dominate and the magnitude of $\phi_a$ begins to decrease. The elastic strain, shown in Fig. Fig. 9(c), tracks the evolution of the stress in Fig. 9(a). All in all, the population based model derived here is capable to predict the main features seen in the response of a thixotropic suspension to a UD-LAOS experiment.

The ability of the model to reasonably predict these experiments suggests the physical models for the kernels provide a reasonable description of the physical reality. These results also provide some validation for the general form of the constitutive equation used in this work.

### *3.4. Comparison with existing structure kinetic models*

The general structure kinetic model in Eq. A.1 [1] and the population based model in Eq. A.2 both involve a single scalar structural variable. In the structure kinetic model, the structural variable $\lambda$ is related to the number of bonds while in the population based model the structural variable $\mu_0$ is related to the aggregation number. In both models, the level of the structural variable depends on the relative strength of aggregation and breakage. Comparing these two expressions, there is no direct mapping possible between the mathematical structure of the two models. This outcome reflects the fundamentally different theoretical bases of the two models, 'bonds' vs 'aggregation number'. As both models capture thixotropic phenomena, the two approaches can be considered complementary.

The population based model possesses some additional attractive features. All the parameters entering the population based model have a microscopic origin, while those in the structure kinetic model equation are purely phenomenological. The emergence of physically meaningful parameters via the population based model demonstrates the benefits of developing a microstructure based model starting from fundamental processes at the particle level using the framework of population balances. In addition, properties of aggregate size distribution underlying the population based model such as aggregate size can, in principle, be measured by independent microstructural measurements such as light and neutron scattering in situ [21, 62]. Therefore, the predictions from the population based model are amenable to independent verification and the work presented here provides a motivation and theoretical framework for such investigations.

## 4. Summary and Conclusions

A coarse grained evolution equation for structure dynamics is developed based on the framework of population balances. This is achieved by incorporating all the relevant physical processes into the rate kernels that describe aggregation-breakage processes. In addition, by accounting for dynamic arrest, the structure evolution equation is applicable to aggregating suspensions with a yield stress and can be combined with a constitutive equation for shear stress to provide rheological predictions.

By fitting to a data set for a published, model thixotropic suspension, it is demonstrated that the population balance based model captures the experimentally measured rheological behavior both qualitatively and quantitatively. This suggests that a single scalar parameter is a reasonable representation of a thixotropic suspension for unidirectional flows. However, comparing the model *predictions* to the flow reversal and LAOS experiments suggests a more accurate constitutive relationship for the elastic stress is needed for better quantitative agreement. These experiments demonstrate that directionality, incorporated into the model through the elastic strain $\gamma_e$, is an important feature of any candidate thixotropic model. Other improvements in the constitutive equation may include incorporating additional, and yet to be accounted for, microscopic variables describing structural anisotropy to facilitate even better agreement with experiments.

The coarse grained model presented in this work represents a significant improvement over simple, highly phenomenological structural models. In addition to incorporating physically meaningful parameters, the microscopic model presented in this work provides a prediction of the aggregation number under shear flow, which is verifiable using independent structural measurements. The phenomenological and ad hoc nature of structure kinetic models precludes such a capability. Therefore the population balance model represents a significant step towards developing better models to describe structural changes in thixotropic suspensions under flow.

Nevertheless, the model remains incomplete. In particular, the coupling of the population balance equation and the stress expression still needs to be derived from more detailed considerations, including satisfying thermodynamic consistency [63]. Such a development will result in a model that is applicable to arbitrary flows beyond simple shear. Furthermore, a more realistic closure approximation can be incorporated such that aggregate polydispersity can be included. These aspects will be explored in a future publication. The immediate utility of the current work is the availability of a microscopically inspired evolution equation for microstructure that may be applied to any existing constitutive relationships for thixotropic suspensions that admit a structural variable.

## 5. Acknowledgements

This material is based upon work supported by the National Science Foundation under Grant No. CBET 312146. Any opinions, findings or recommendations expressed in this material are those of the author(s) and do not necessarily reflect the views of the National Science Foundation.

Table 2: Nomenclature

| Symbol | Variable |
|---|---|
| $\alpha$ | Collision efficiency |
| $\beta$ | Cut-off function |
| $\dot{\gamma}$ | Shear rate |
| $\eta_r^h$ | Relative suspension viscosity |
| $\gamma_{lin}$ | Equilibrium limiting strain |
| $\gamma_e$ | Elastic strain |
| $\lambda$ | Structure parameter |
| $\mu_s$ | Medium viscosity |
| $\mu_k$ | k$^{th}$ scaled moment |
| $\mu_0$ | Reciprocal of aggregation number |
| $\phi_a$ | Aggregate volume fraction |
| $\phi_{max}$ | Maximum packing fraction |
| $\phi_p$ | Total solids loading |
| $\phi_{pc}$ | Primary cluster volume fraction |
| $\phi_v$ | Viscometric volume fraction |
| $\theta_o$ | Number of fragments |
| $a_p$ | Primary particle radius |
| $a_{pc}$ | Primary cluster radius |
| $b_o$ | Breakage coefficient |
| $d$ | Breakage exponent |
| $d_f$ | Aggregate fractal dimension |
| $d_{fpc}$ | Cluster fractal dimension |
| $G_{eq}$ | Equilibrium modulus |
| $k_B$ | Boltzmann's contant |
| $m$ | Number of primary particles in aggregate |
| $m_p$ | Number of primary particles in primary cluster |
| $M_k$ | k$^{th}$ moment |
| $\hat{n}(x)$ | Scaled number density |
| $n(x)$ | Number density of parimary particles |
| $N_o$ | Number of primary particles |
| $P(m\|q)$ | Daughter distribution |
| $P(\xi)$ | Self-similar daughter distribution |
| $R_g$ | Radius of gyration |
| $R_h$ | Hydrodynamic radius |
| $R_h/R_a$ | Aggregate porosity |
| $T(298K)$ | Temperature |
| $W$ | Stability ratio |

## Appendix A. The structure kinetic approach

The primary feature of many thixotropy models is the dependence of material properties on the structure parameter, $\lambda$, which defines the state of the system under non-equilibrium conditions. This class of structure kinetic models follow from the work of Goodeve [15] and can generically be represented by

$$\frac{d\lambda}{dt} = -k_1\dot{\gamma}^{k_2}\lambda^{k_3} + k_4(1-\lambda)^{k_5} + k_6\dot{\gamma}^{k_7}(1-\lambda)^{k_8} \ , \qquad \text{(A.1)}$$

where $\dot{\gamma}$ is the shear rate. The rate equation for $\lambda$ accounts for contributions to microstructure evolution by shear breakage, Brownian aggregation and shear aggregation. These are represented, respectively, by the first, second and third terms on the right hand side of Eq. A.1 and involve pre-factors and exponents as fit parameters.

For comparison, the population based model in Eq. 26 can be re-expressed in a similar form involving only generic kinetic coefficients as

$$\begin{aligned} \frac{d\mu_0}{dt} =& k_1|\dot{\gamma}|^2\left(\mu_0^{1-1/d_f} - m_p^{1/d_{fpc}}\mu_0\right) - k_2\mu_0^2 - k_3|\dot{\gamma}|\mu_0^{2-3/d_f} \ , \\ & with \\ & k_1 = b_o\left(\theta_0 - 1\right) \ , \\ & k_2 = 2\beta\left(\frac{kT\phi_p}{2\mu_s\eta_r^h W\pi a_p^3}\right) \ and \\ & k_3 = 4\beta\alpha\left(\frac{\phi_p}{\pi}\right) \ . \end{aligned} \qquad \text{(A.2)}$$

The three terms on the right hand side of the evolution equation for $\mu_0$ also account for shear breakage, Brownian aggregation and shear aggregation respectively.

## References


[1] Mewis J, Wagner NJ. *Colloidal suspension rheology.* Cambridge: Cambridge University Press, 2012.

[2] Hoffmann H, Rauscher A. Aggregating systems with a yield stress value. *Colloid Polym Sci.* 1993;271:390–395.

[3] Bird RB, Marsh BD. Viscoelastic hysteresis. Part I. Model predictions. *T Soc Rheol.* 1968;12:479-488.

[4] Ruckenstein E, Mewis J. Kinetics of structural changes in thixotropic fluids. *J Colloid Interface Sci.* 1973;44:532–541.

[5] Mewis J. Thixotropy-a general review. *J Non-Newton Fluid.* 1979;6:1–20.

[6] Barnes HA. Thixotropy-a review. *J Non-Newton Fluid.* 1997;70:1 - 33.

[7] Mewis J, Wagner NJ. Thixotropy. *Adv Colloid Interface Sci.* 2009;147:214–227.

[8] Boger DV. Rheology and the resource industries. *Chem Eng Sci.* 2009;64:4525–4536.

[9] Chang C, Smith PA. Flow-induced structure in a system of nuclear waste simulant slurries. *Rheol Acta.* 1996;35:382–389.

[10] Thareja P, Golematis A, Street CB, et al. Influence of surfactants on the rheology and stability of crystallizing fatty acid pastes. *J Am Oil Chem Soc.* 2013;90:273–283.

[11] Natan B, Rahimi S. The status of gel propellants in year 2000. *Int J Energetic Materials Chem Prop.* 2002;5.

[12] Green H, Weltmann R. Analysis of Thixotropy of Pigment-Vehicle Suspensions-Basic Principles of the Hysteresis Loop. *Ind Eng Chem.* 1943;15:201–206.

[13] Hahn SJ, Ree T, Eyring H. Flow mechanism of thixotropic substances. *Ind Eng Chem.* 1959;51:856–857.

[14] Apostolidis AJ, Armstrong MJ, Beris AN. Modeling of human blood rheology in transient shear flows. *J Rheol.* 2015;59:275-298.

[15] Goodeve CF. A general theory of thixotropy and viscosity. *Trans. Faraday Soc.*. 1939;35:342–358.

[16] Dullaert K, Mewis J. A structural kinetics model for thixotropy. *J Non-Newton Fluid.* 2006;139:21 - 30.

[17] Randolph AD, Larson MA. Transient and steady state size distributions in continuous mixed suspension crystallizers. *AIChE J.* 1962;8:639–645.

[18] Hulburt HM, Katz S. Some problems in particle technology: A statistical mechanical formulation. *Chem Eng Sci.* 1964;19:555–574.

[19] Von Smoluchowski M. Versuch einer mathematischen theorie der koagulationskinetik kolloider lösungen. *Zeit Phys Chem.* 1917;92:129-168.

[20] Flesch Jürgen C, Spicer PT, Pratsinis SE. Laminar and turbulent shear-induced flocculation of fractal aggregates. *AIChE J.* 1999;45:1114–1124.

[21] Spicer P, Pratsinis SE. Coagulation and fragmentation: Universal steady-state particle-size distribution. *AIChE J.* 1996;42:1612–1620.

[22] Von Smoluchowski M. Three discourses on diffusion, Brownian movements, and the coagulation of colloid particles. *Phys. Z. Sowjet.* 1916;17:557–571.

[23] Barthelmes G, Pratsinis SE, Buggisch H. Particle size distributions and viscosity of suspensions undergoing shear-induced coagulation and fragmentation. *Chem Eng Sci.* 2003;58:2893-2902.

[24] Mohtaschemi M, Puisto A, Illa X, Alava MJ. Rheology dynamics of aggregating colloidal suspensions. *Soft matter.* 2014;10:2971–2981.

[25] Armstrong MJ, Beris AN, Rogers SA, Wagner NJ. Dynamic shear rheology of a thixotropic suspension: Comparison of an improved structure-based model with large amplitude oscillatory shear experiments. *J Rheol.* 2016;60:433-450.

[26] Dullaert K, Mewis J. A model system for thixotropy studies. *Rheol Acta.* 2005;45:23–32.

[27] Meakin Paul. Fractal aggregates. *Adv Colloid Interface Sci.* 1987;28:249–331.

[28] Ramkrishna D. *Population balances: Theory and applications to particulate systems in engineering*. San Diego, CA: Academic Press, 2000.

[29] Fuchs N. Über die Stabilität und Aufladung der Aerosole. *Z Phys.* 1934;89:736–743.

[30] Thomas DN, Judd SJ, Fawcett N. Flocculation modelling: a review. *Water Res.* 1999;33:1579–1592.

[31] Marchisio DL, Fox RO. *Computational models for polydisperse particulate and multiphase systems*. Cambridge: Cambridge University Press, 2013.

[32] Diemer RB, Olson JH. A moment methodology for coagulation and breakage problems: Part 1-analytical solution of the steady-state population balance. *Chem Eng Sci.* 2002;57:2193 - 2209.

[33] Diemer RB, Olson JH. A moment methodology for coagulation and breakage problems: Part 2-moment models and distribution reconstruction. *Chem Eng Sci.* 2002;57:2211 - 2228.

[34] Sommer M, Stenger F, Peukert W, Wagner NJ. Agglomeration and breakage of nanoparticles in stirred media millsa comparison of different methods and models. *Chem Eng Sci.* 2006;61:135–148.

[35] Kruis FE, Kusters KA, Pratsinis SE, Scarlett B. A simple model for the evolution of the characteristics of aggregate particles undergoing coagulation and sintering. *Aerosol Sci Technol.* 1993;19:514–526.

[36] Vemury S, Kusters KA, Pratsinis SE. Time-lag for attainment of the self-preserving particle size distribution by coagulation. *J Colloid Interface Sci.* 1994;165:53–59.

[37] Dullaert K, Mewis J. Stress jumps on weakly flocculated dispersions: Steady state and transient results. *J Colloid Interface Sci.* 2005;287:542 - 551.

[38] Lewis TB, Nielsen LE. Viscosity of dispersed and aggregated suspensions of spheres. *T Soc Rheol.* 1968;12:421–443.

[39] Russel WB, Wagner NJ, Mewis J. Divergence in the low shear viscosity for Brownian hard-sphere dispersions: At random close packing or the glass transition? *J Rheol.* 2013;57:1555–1567.

[40] Faroughi SA, Huber C. A generalized equation for rheology of emulsions and suspensions of deformable particles subjected to simple shear at low Reynolds number. *Rheol Acta.* 2015;54:85–108.

[41] Maron SH, Pierce PE. Application of Ree-Eyring generalized flow theory to suspensions of spherical particles. *J Colloid Sci.* 1956;11:80–95.

[42] Dullaert K. Constitutive Equations for Thixotropic Dispersions, Ph.D.

Thesis, Katholieke Universiteit Leuven, Leuven, Belgium, 2005.

[43] Armstrong M. Investigating and modeling thixotropic behavior, microstructure and rheology of complex material, Ph.D. Thesis, University of Delaware, Newark, Delaware, 2015.

[44] Potanin AA, De Rooij R, Ende D, Mellema J. Microrheological modeling of weakly aggregated dispersions. *J Chem Phys.* 1995;102:5845-5853.

[45] Hsiao LC, Newman RS, Glotzer SC, Solomon MJ. Role of isostaticity and load-bearing microstructure in the elasticity of yielded colloidal gels. *Proceedings of the National Academy of Sciences.* 2012;109:16029–16034.

[46] Russel WB. Theoretical approaches to the rheology of concentrated dispersions. *Powder Technol.* 1987;51:15–25.

[47] Shih WH, Shih WY, Kim SI, Liu J, Aksay IA. Scaling behavior of the elastic properties of colloidal gels. *Phys Rev A.* 1990;42:4772.

[48] Dimitriou CJ, Ewoldt RH, McKinley GH. Describing and prescribing the constitutive response of yield stress fluids using large amplitude oscillatory shear stress (LAOStress). *J Rheol.* 2013;57:27-70.

[49] Armstrong MJ, Beris AN, Wagner NJ. An Adaptive Parallel Tempering Method for the Dynamic Data-Driven Parameter Estimation of Nonlinear Models (submitted). *AIChE J.* 2016.

[50] Curtis ASG, Hocking LM. Collision efficiency of equal spherical particles in a shear flow. The influence of London-van der Waals forces. *Trans. Faraday Soc.*. 1970;66:1381-1390.

[51] Riseman J, Kirkwood JG. The Intrinsic Viscosity, Translational and Rotatory Diffusion Constants of Rod-Like Macromolecules in Solution. *J Chem Phys.* 1950;18:512–516.

[52] Meakin P, Chen ZY, Deutch JM. The translational friction coefficient and time dependent cluster size distribution of three dimensional cluster–cluster aggregation. *J Chem Phys.* 1985;82:3786–3789.

[53] Lattuada M, Wu H, Morbidelli M. Hydrodynamic radius of fractal clusters. *J Colloid Interface Sci.* 2003;268:96–105.

[54] Weitz DA, Huang JS, Lin MY, Sung J. Limits of the fractal dimension for irreversible kinetic aggregation of gold colloids. *Phys Rev Lett.* 1985;54:1416.

[55] Oles V. Shear-induced aggregation and breakup of polystyrene latex particles. *J Colloid Interface Sci.* 1992;154:351–358.

[56] Reerink H, Overbeek JG. The rate of coagulation as a measure of the stability of silver iodide sols. *Discuss Faraday Soc.* 1954;18:74–84.

[57] Russel WB, Saville DA, Schowalter WR. *Colloidal dispersions.* Cambridge: Cambridge University Press, 1992.

[58] Adler PM, Mills PM. Motion and Rupture of a Porous Sphere in a Linear Flow Field. *J Rheol.* 1979;23:25-37.

[59] Sonntag RC, Russel WB. Structure and breakup of flocs subjected to fluid stresses: II. Theory. *J Colloid Interface Sci.* 1987;115:378 - 389.

[60] Higashitani K, Iimura K. Two-Dimensional Simulation of the Breakup Process of Aggregates in Shear and Elongational Flows. *J Colloid Interface Sci.* 1998;204:320 - 327.

[61] Harshe YM, Lattuada M. Breakage Rate of Colloidal Aggregates in Shear Flow through Stokesian Dynamics. *Langmuir.* 2012;28:283-292. PMID: 22122803.

[62] Sandkühler P, Sefcik J, Lattuada M, Wu H, Morbidelli M. Modeling structure effects on aggregation kinetics in colloidal dispersions. *AIChE J.* 2003;49:1542–1555.

[63] Larson RG. Constitutive equations for thixotropic fluids. *J Rheol.* 2015;59:595–611.